Fast and Accurate Quantification of Elemental Macrosegregation in Continuously Cast Slabs Using the Micro-XRF Technique

Macrosegregation adversely affects the mechanical performance of continuously cast steel slabs. Micro-x-ray fluorescence with a 20 µm spot size enables rapid elemental analysis. This study investigates the spatial distribution of manganese, silicon and aluminum in thin-slab caster samples using a Bruker M4 Tornado system. The combination of fundamental parameter calibration and quantification of pixels within the map processing enabled accurate quantification of elemental variations. The results were further validated through multiscale analyses using confocal laser scanning microscopy and scanning electron microscopy. The optimized methodology provides an efficient and reliable approach for quantitative segregation assessment.

Authors

Muhammad Anwarul Nazim (top left), Metallurgical Engineer, U. S. Steel Research and Technology Center, Munhall, Pa., USA

Thinium Natarajan, Research Engineer, U. S. Steel Research and Technology Center, Munhall, Pa., USA
ttnatarajan@uss.com

Scott Story (top right), Senior Research Consultant, Enterprise Process Innovation, U. S. Steel Research and Technology Center, Munhall, Pa., USA
srstory@uss.com

Ronald O'Malley (bottom), F. Kenneth Iverson Chair Professor and Director, Peaslee Steel Manufacturing Research Center, Department of Material Science and Engineering, Missouri University of Science and Technology, Rolla, Mo., USA
omalleyr@mst.edu

Introduction

Modern steel development increasingly relies on higher alloying additions, especially in advanced high-strength steel grades, to achieve enhanced mechanical performance, particularly in terms of strength and ductility. During solidification, alloying elements are preferentially rejected at the advancing solid–liquid interface, enriching the interdendritic liquid and causing the final liquid to solidify to become highly solute-rich. This enrichment initially leads to microsegregation, which occurs over a small length scale as solute partitions locally between dendrite arms. In contrast, macrosegregation is an inherent consequence of solute redistribution during the solidification of continuously cast steel slabs and occurs at the scale of the casting when this microsegregated, solute-enriched liquid is transported by fluid flow and solidification-induced phenomena to the final regions of solidification.[1] The accumulation of enriched liquid and dendrite fragments in these regions promotes large-scale chemical inhomogeneities, among which centerline segregation is particularly detrimental in continuously cast slabs, as it can persist through downstream processing and degrade mechanical performance. Areas with pronounced centerline segregation commonly act as preferential crack initiation sites due to localized differences in grain structure and mechanical behavior. In highly alloyed steels, severe centerline enrichment can also trigger the unintended formation of brittle martensitic microstructures during subsequent heat treatment, increasing susceptibility to fracture and fatigue failure during service.[2]

Precise quantitative measurement plays a central role in ensuring effective process control and consistent product quality; nevertheless, developing a dependable approach for quantitatively assessing centerline segregation in as-cast steel has remained a persistent challenge within the steel industry.[3–5] Historically, methods for evaluating centerline segregation in continuously cast steel can be broadly classified according to the nature of the information they provide, ranging from qualitative visual assessment to localized chemical quantification.[3,4] The most widely used industrial approach remains macro-etch-based visual comparison, typically referenced to Mannesmann charts.[6] Another widely used industrial method is the Norme Française AFNOR (NFA) rating system, which employs 2% Nital etching followed by surface evaluation using comparative

scoring charts.[7] Sulfur printing, in which sulfur distribution can be visualized by first immersing photographic paper in a dilute acidic solution and then pressing it against a properly prepared steel surface, allows regions with elevated sulfur content to be identified.[3] While these methods are simple and inexpensive, they rely heavily on operator judgment and etch quality, leading to poor reproducibility and limited sensitivity, particularly for distinguishing slabs with relatively low but metallurgically significant segregation levels. Moreover, wet chemistry-based carbon drilling evaluates segregation by sampling drilled cores at multiple locations and measuring carbon content using standard analyses, but the need for extensive drilling leads to limited spatial resolution and slow turnaround along with its destructive nature.[5,8]

To reduce subjectivity, image-based techniques have been proposed in which macro-etched slab images are digitally processed to extract geometric features such as area fraction, continuity or characteristic length of segregated regions.[4] Although these approaches improve repeatability compared to purely visual rating, they remain dependent on etching contrast and surface condition. Because the extracted features reflect optical morphology rather than direct chemical information, even advanced image-processing and deep-learning methods provide only an indirect assessment of segregation severity and cannot reliably quantify elemental enrichment or distinguish between steels with similar etched appearance but different levels of segregation.[9]

In contrast, chemical analysis techniques such as optical emission spectroscopy (OES), electron probe microanalysis (EPMA), computer-aided microanalysis (CMA) and laser-induced breakdown spectroscopy (LIBS) provide direct information on elemental enrichment at the slab centerline and enable segregation to be expressed in terms of local-to-bulk concentration ratios. While these methods offer higher scientific rigor, their application is often constrained by destructive sample preparation, limited spatial coverage and, depending on the technique, extended analysis times (except LIBS), which can limit practicality for routine use in a production environment. Furthermore, the criteria used to quantify segregation severity are frequently element- and grade-specific, complicating the establishment of a universal segregation metric.[4]

Laser ablation–inductively coupled plasma mass spectrometry (LA-ICP-MS) has been applied for quantitative evaluation of macrosegregation in continuously cast steel slabs, offering high elemental sensitivity and fine spatial resolution through line-based analysis. The technique can resolve local enrichment of alloying elements such as Mn and Nb; however, its inherently one-dimensional nature makes segregation severity highly dependent on scan placement relative to heterogeneous segregation features. As a result, banded or discontinuous segregation may be under- or overrepresented. In addition, LA-ICP-MS is destructive and requires specialized instrumentation and calibration, limiting its suitability for rapid, large-area, two-dimensional segregation assessment in industrial environments.[10]

Energy-dispersive x-ray spectroscopy (EDS) coupled with scanning electron microscopy (SEM) is widely employed for elemental analysis in steels by detecting characteristic x-rays generated through electron excitation. While SEM-EDS is effective for localized, semiquantitative measurements — particularly for light elements — it is limited by relatively high detection limits and reduced peak resolution for heavier alloying elements, as well as by its inherently small analysis area.[5] Consequently, mapping centerline segregation over large slab cross-sections requires extensive sample preparation and analysis of numerous discrete specimens, rendering the approach labor-intensive and impractical for routine, spatially representative segregation evaluation.

Defect detection in steel is also performed by density measurements, optical microscopy, radiographic imaging (x-ray or gamma ray), eddy current testing and ultrasonic inspection. These methods effectively identify pores, cracks, inclusions and centerline porosity, often requiring specialized equipment and expertise. However, while they detect defects associated with segregation, they do not directly measure solute segregation.[3]

More recently, synchrotron micro-x-ray fluorescence (SMXRF) has demonstrated the ability to generate high-resolution, large-area compositional maps of centerline segregation by exploiting the exceptionally high photon flux available at synchrotron facilities. Despite its analytical power, SMXRF is constrained by limited access to synchrotron beam time, long experimental lead times and reduced sensitivity to heavier elements in iron-rich matrices due to attenuation effects, confining its application largely to fundamental research rather than industrial practice.[11]

In contrast, laboratory-based micro-x-ray fluorescence (micro-XRF) offers a practical alternative that combines spatially resolved chemical mapping with industrial feasibility. By employing a focused x-ray beam with spot sizes on the order of tens of micrometers, micro-XRF enables rapid, nondestructive elemental mapping over relatively large areas with minimal sample preparation. Unlike SEM-EDS or EPMA, micro-XRF provides superior detection limits for heavier alloying elements and improved peak resolution at higher x-ray energies, making it particularly well suited for quantitative characterization of centerline segregation in steel slabs.[5] Although quantitative micro-XRF analysis must account for matrix effects, absorption and interelement fluorescence — especially for lighter elements such as Si and Al in iron-rich matrices — its balance of chemical sensitivity, spatial coverage and practicality positions micro-XRF as a bridging technique between high-resolution research tools and production-relevant segregation assessment.

To address these issues, fundamental parameter (FP)–based quantification has been adopted to measure

macrosegregation of Mn on steel slabs.[12,13] The FP approach relies on well-established physical constants governing x-ray generation and absorption and iteratively refines elemental compositions until simulated spectra match experimental measurements. When combined with appropriate correction factors, FP quantification can significantly improve accuracy in heterogeneous materials. In addition, the choice of scan parameters, including step size and pixel binning, plays a critical role in balancing spatial resolution, measurement time and quantitative reliability. However, systematic studies identifying optimal micro-XRF scanning strategies for segregation characterization in steel slabs remain limited.

The present work addresses these gaps by developing a micro-XRF-based methodology for quantitative characterization of macrosegregation in continuously cast steel slabs, with particular emphasis on manganese, silicon and aluminum distributions. Using a Bruker M4 Tornado micro-XRF system, this study systematically evaluates the influence of step size and pixel binning on elemental quantification accuracy and measurement efficiency. By applying FP-based calibration in combination with the quantification of pixels within the map (QMAP) approach, spatially resolved elemental distributions are quantified and validated against optical emission spectroscopy measurements. The results establish optimized scanning conditions that enable rapid, nondestructive and accurate segregation analysis, providing a practical framework for both research and industrial setting, and are further corroborated through complementary confocal laser scanning microscope (CLSM) and SEM-EDS analyses demonstrating consistent identification of Mn–S segregation.

Theoretical Background

X-ray fluorescence (XRF) analysis is based on the excitation and relaxation of inner-shell electrons in atoms exposed to high-energy x-ray irradiation. When an incident x-ray photon ionizes an inner atomic shell, the resulting vacancy is rapidly filled by an electron from a higher energy level, leading to the emission of characteristic x-ray photons with energies that are unique to each element. Because these electronic transitions occur between quantized inner-shell energy levels, the emitted fluorescence lies in the x-ray energy range and serves as a direct fingerprint of elemental composition rather than chemical bonding. By detecting the energy of the emitted photons using energy- or wavelength-dispersive methods, individual elements can be identified qualitatively, while counting the number of photons allows the quantitative determination of elemental concentrations as illustrated in the schematics of Fig. 1, forming the physical basis of micro-XRF for spatially resolved analysis of heterogeneous metallic materials, like steels.

Micro-XRF with polycapillary lenses offers significant advantages, including substantially reduced spot excitation, enhanced spatial resolution and high local photon flux. In this approach, primary x-rays emitted from the source are collected over a large solid angle and guided through the polycapillary lens by multiple total external reflections. The lens concentrates the polychromatic x-ray beam into a small focal spot on the sample surface, independent of the x-ray tube focal size. This concentration increases excitation efficiency while limiting the interaction volume, which is critical for resolving fine chemical heterogeneities. Fig. 2 schematically illustrates the excitation–detection geometry, where the focused beam generates localized fluorescence that is collected by the detector at an oblique take-off angle.

In micro-XRF quantification, the improved spatial resolution enabled by polycapillary focusing must be balanced against counting statistics and total acquisition time. As illustrated in Fig. 3, the total measurement time is governed by the dwell time per pixel, the pixel size and the scanned area. Increasing dwell time improves counting statistics and quantitative precision, particularly for minor and trace elements, while smaller pixel sizes enhance spatial resolution at the cost of reduced counts per pixel. Similarly, larger scan areas improve representativeness for heterogeneous materials but proportionally increase total measurement time. Consequently, reliable micro-XRF quantification requires optimizing these parameters to achieve an appropriate compromise between spatial resolution, statistical accuracy and experimental efficiency.

Following the optimization of acquisition parameters, elemental concentrations in micro-XRF are commonly determined using the FP quantification method.[12,13]

Figure 1

Schematics of the working principle of x-ray fluorescence to quantify all the chemical elements in a sample.

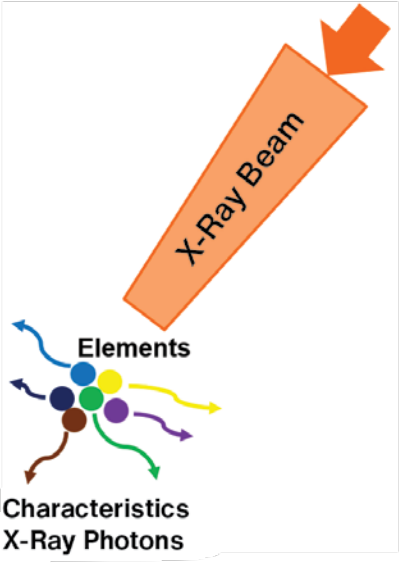

Figure 2

Schematics of polycapillary lenses-focused micro-x-ray fluorescence (XRF) geometry.

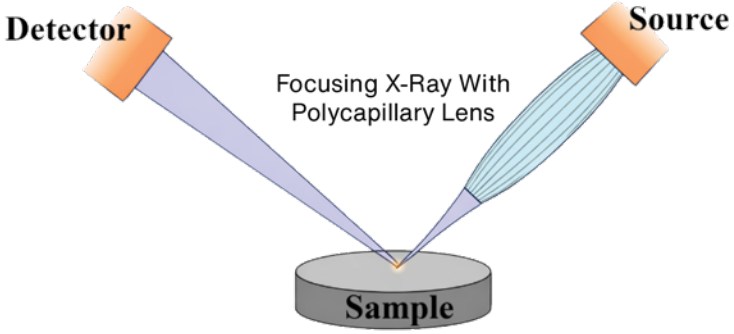

Figure 3

Key parameters governing micro-XRF measurement time.

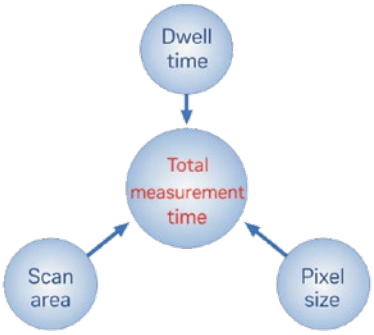

In this approach, measured fluorescence intensities are interpreted using physically based models that describe x-ray excitation, fluorescence generation, absorption and secondary enhancement effects within the sample matrix. The FP method incorporates instrument-specific factors such as excitation spectrum, detector efficiency, measurement geometry and polycapillary lens transmission to calculate theoretical line intensities. Elemental concentrations are then obtained by iteratively adjusting the composition until calculated and measured intensities converge. This physics-based framework enables quantitative analysis without extensive calibration standards, while remaining sensitive to measurement conditions and sample heterogeneity.

Within the fundamental parameters model, an assumed sample composition is iteratively refined, while the resulting fluorescence spectrum is forward-computed by repeatedly solving a form of the Sherman equation:[14]

$$I_{fl} = C_i \cdot K_i \cdot \int_{E_{abs,i}}^{E_{\max}} I_o(E) \cdot \tau_{i,E} \cdot Q_i(E, E_{fl}) \cdot \frac{1}{\mu^*} dE \quad \text{(Eq. 1)}$$

The FP model is based on Eq. 1, which uses intensity I_{fl} to quantify samples. The model accounts for excitation spectrum $I_o(E)$, attenuation of the incident x-ray beam as it penetrates the sample and attenuation of the emitted fluorescence radiation as it exits the material, both described by the effective mass attenuation coefficient μ^* which includes absorption and scattering effects. Sample composition C_i, instrument sensitivity for the respective element K_i and atomic parameters — namely the photoionization cross-section and fluorescence yield, represented by the combined photo-absorption and photon production term $\tau_{i,E} \cdot Q_i(E,E_{fl})$ — are also explicitly incorporated.

Building on this formulation, the FP framework employs an iterative solution in which elemental concentrations are systematically adjusted until the calculated fluorescence intensities converge with the measured values. In this process, deviations between modeled and experimental spectra are minimized through repeated forward calculations that consistently apply the physical parameters described earlier. This physics-based approach enables quantitative interpretation of XRF data without requiring extensive empirical calibration, while still allowing the inclusion of correction factors to account for instrument-specific or sample-related effects. As a result, the FP method provides a robust theoretical foundation for quantitative micro-XRF analysis, particularly for compositionally complex and heterogeneous materials.

Experimental: Materials, Equipment and Procedures

Materials and Reference Measurements

Thin-slab steel samples representative of advanced high-strength steel (AHSS) grades were investigated. Multiple samples (TS1-2 × 2, TS12 and MN1) containing varying levels of manganese, silicon and aluminum were selected to evaluate the robustness of the micro-XRF quantification approach across different chemical compositions. The analyzed regions included slab mid-thickness sections where centerline segregation is typically most pronounced. Samples were surface-finished by a milling machine prior to the analysis. Fig. 4a shows the surface of a thin-slab steel sample after milling, highlighting the analyzed region at the slab mid-thickness. The left image presents an overview of the scanned surface in the form of a mosaic image of the sample, while the highlighted and magnified region corresponds to the area over which spatially resolved micro-XRF measurements were performed to capture local chemical variations associated with segregation.

Optical emission spectroscopy (OES) was used as the reference method for quantitative validation. As shown

Figure 4

Representative thin-slab steel sample (TS1-2 × 2) and analyzed regions used for micro-XRF and reference measurements: A mosaic image of the milled slab mid-thickness surface, with a magnified view highlighting the area (24 mm x 21 mm) of measured micro-XRF scan (a); and the sample's optical emission spectroscopy (OES) reference measurements, with marked locations indicating measurement points aligned with the micro-XRF scan paths on the opposite face of the samples (b).

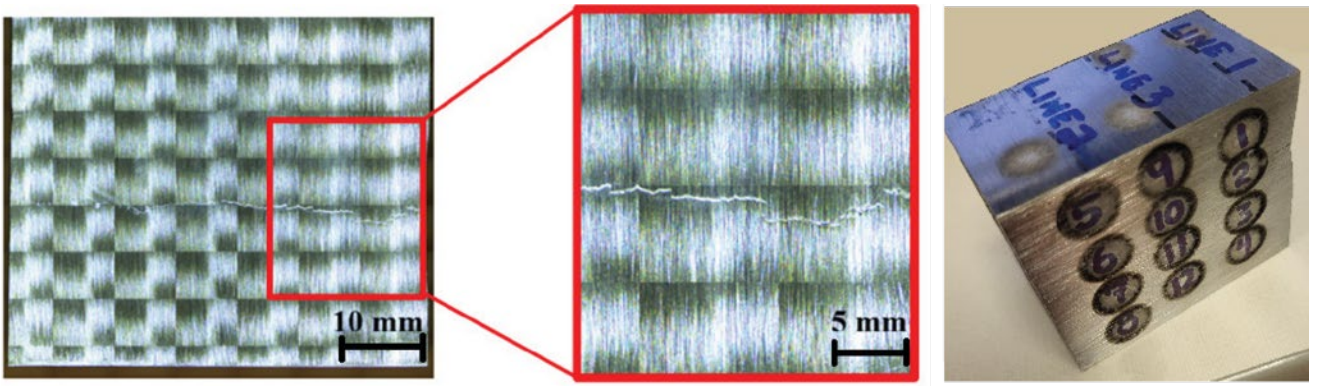

(a) (b)

Table 1

Key Technical Specifications of the Micro-XRF Device of Bruker M4 Tornado

MXRF component	Technical specifications
Excitation source	Micro-focus or fine-focus x-ray tube; maximum accelerating voltage 50 kV; tube power up to 40 W; Rhodium (Rh) anode
X-ray optics	Polycapillary x-ray lens enabling focused excitation; optional collimators with diameters up to 2 mm
Detector	Silicon drift detector (SDD); single 30 mm^2 or 60 mm^2; energy resolution ≤145 eV (Mn Kα)
Maximum count rate	Up to 300 kcps (single SDD); higher effective count rate with dual SDD configuration
Spot size	Minimum ~20 µm with polycapillary optics; up to ~2 mm using collimators
Step size	Minimum programmable scan step size ≈ 4 µm
Measurement medium	Air or vacuum operation
Vacuum system	Integrated vacuum system; chamber pressure down to ~20 mbar
Sample types	Bulk solids, coatings, powders, particles, and heterogeneous materials
Sample stage	Motorized X–Y–Z translation stage
Stage travel range	200 mm × 160 mm × 120 mm
Maximum mapping area	Up to 190 mm × 160 mm
Maximum sample weight	Up to 5 kg
Optical imaging	Dual optical cameras with 10X and 100X magnification; automated image stitching and mosaic generation
Software and control	Integrated Bruker M4 software for instrument control, spectral acquisition, elemental mapping and quantitative analysis

in Fig. 4b, OES measurements were performed at multiple marked locations along lines spatially aligned with the micro-XRF scan paths on the opposite side of the samples, enabling direct point-by-point comparison between the two techniques. Average compositions and local compositional variations obtained from OES were used to assess the accuracy and robustness of the micro-XRF quantification across samples with varying Mn, Si, and Al contents.

Equipment: Micro-XRF – Bruker M4 Tornado

The micro-XRF measurements were carried out using a Bruker M4 Tornado high-performance micro-XRF spectrometer, as shown in Fig. 5. The instrument is an energy-dispersive x-ray fluorescence system designed for spatially resolved elemental analysis of bulk materials, coatings and heterogeneous microstructures. The key technical specifications of the unit are shown in Table 1.

Fig. 5a shows the fully enclosed, radiation-shielded Bruker M4 Tornado micro-XRF spectrometer with integrated excitation source, detection system, motorized sample stage, vacuum system and software-controlled operation. As shown in Fig. 5b, samples are mounted on a motorized X–Y–Z translation stage, enabling precise positioning and automated point, line-scan, and area-mapping measurements, with excitation from above and fixed detector geometry.

Figure 5

Micro-XRF instrumentation and measurement geometry used in this study: Bruker M4 Tornado micro-XRF spectrometer showing the enclosed measurement chamber and human-machine interface (HMI) (a); interior view of the sample chamber illustrating the motorized sample stage, sample position and fixed detector–optics assembly (b); and schematic representation of the x-ray excitation and detection principle, showing the Rh-anode x-ray tube, primary filters, polycapillary optics focusing the beam to a localized spot on the sample and fluorescence detection geometry under controlled atmospheric conditions (c).

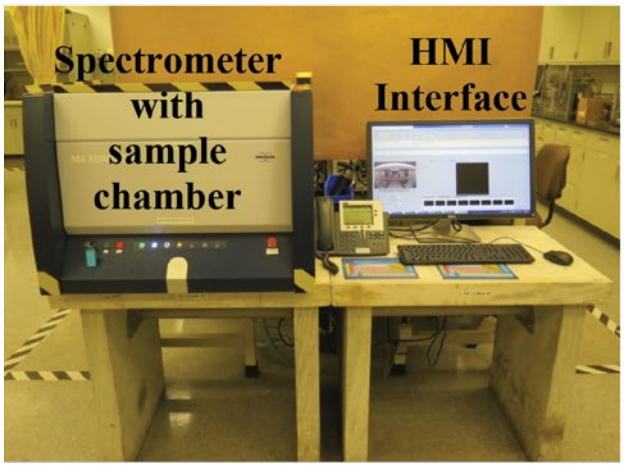

(a)

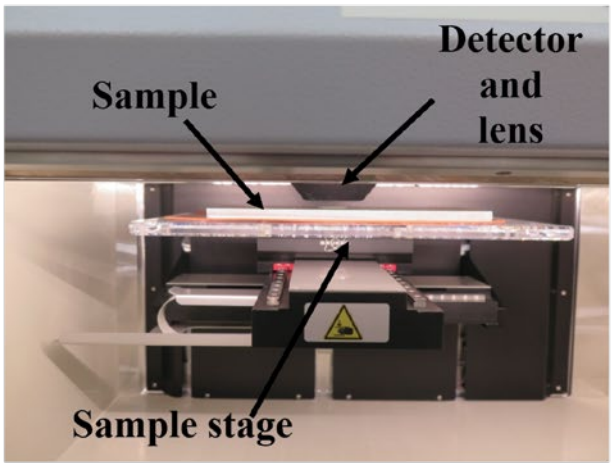

(b)

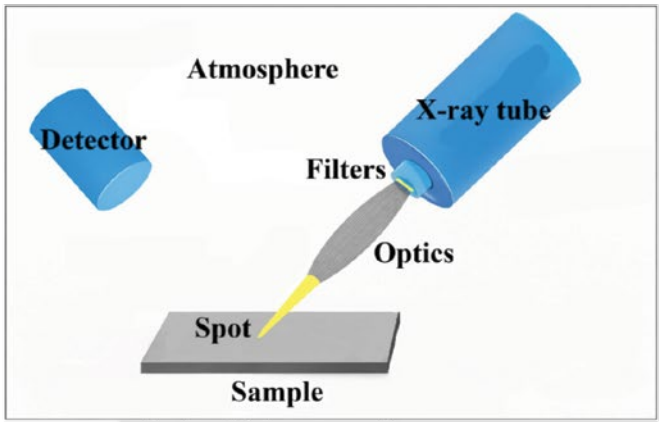

(c)

Fig. 5c illustrates the excitation and detection principle. X-ray fluorescence is excited using a micro-focus or fine-focus Rh-anode x-ray tube. The beam is spectrally conditioned using filters and focused by polycapillary optics. Fluorescence is detected by silicon drift detector (SDD). Measurements were performed under reduced pressure (~20 mbar) to minimize air absorption effects for improved analysis of elements like silicon and aluminum.

QMAP and FP Quantification

Elemental maps were acquired over representative regions using step sizes of 10, 20 and 50 µm, while maintaining a fixed x-ray spot size of 20 µm. Quantitative elemental mapping was performed using the Quantification of Elemental Area Distribution Map (QMAP) module within the Bruker software. During map acquisition, a pixel dwell time of 10 ms and a stage speed of 2 mm/second were used. The x-ray tube was operated at 50 kV and 150 µA, which maintained the system dead time below 50%. Throughout the experiments, the measurement chamber was held at an air pressure of 20 mbar.

The QMAP approach enables pixel-by-pixel quantification across the entire scanned area. To assess the effects of signal averaging and noise reduction on quantitative accuracy, pixel binning configurations of 1 × 1, 3 × 3, 5 × 5 and 9 × 9 were applied during QMAP processing. Elemental concentrations were calculated using a FP–based quantification model, which iteratively simulates XRF spectra based on known interaction probabilities and refines elemental compositions until convergence. For lighter elements, such as silicon and aluminum, additional FP correction factors were applied to account for matrix effects and inter-element fluorescence interactions. A vacuum environment was employed during measurement to improve quantification accuracy for low-Z elements.

In a separate experimental study, concentric solidification samples produced using a CLSM were analyzed using the Bruker M4 micro-XRF system to further validate elemental quantification. During concentric solidification, manganese and sulfur precipitate as MnS into the remaining liquid that remains in the final stages of solidification. The measured manganese and sulfur concentrations were compared with corresponding results obtained from SEM-EDS analysis. Concentric solidification is a controlled technique in which solidification progresses radially from the outer surface toward the center, generating nearly concentric solid–liquid interfaces under well-defined thermal conditions. The detailed procedure of the concentric solidification experiment is beyond the scope of the present work.

Table 2

Mean and Standard Deviation (std) of Mn and Si (wt. %) From Repeated OES Measurements Along Two Lines in TS1-2 × 2 Sample

Line	Mn mean [wt. %]	Mn std [wt. %]	Si mean [wt. %]	Si std [wt. %]
1	2.700	0.008	2.025	0.039
2	2.695	0.013	2.003	0.043

Results and Discussion

Effect of Step Size and Pixel Binning on Elemental Quantification

Table 2 presents repeated OES measurements acquired along two independent lines in the first TS1-2 × 2 sample, focusing exclusively on manganese and silicon, while other trace elements were excluded. Manganese shows excellent repeatability, with mean values of 2.700 wt. % (Line 1) and 2.695 wt. % (Line 2) and very low standard deviations (<0.02 wt. %). Silicon exhibits slightly higher scatter, with standard deviations of ~0.04 wt. %, but remains consistent between the two lines. The small line-to-line differences are within experimental uncertainty, confirming that the OES data provide a stable and reliable reference for validating micro-XRF quantification.

Micro-XRF spectrum acquisition of the milled TS1-2 × 2 sample surface was conducted on the mosaic image using area scans with step sizes of 10, 20 and 50 µm. A 24 mm × 21 mm region of the sample was selected from the mosaic image for subsequent quantitative analysis. Subsequently, QMAP was used to perform pixel-by-pixel quantification of elemental concentrations across the entire mapped region. Table 3 shows the time required to measure, QMAP process the scanned area of the representative regions using step sizes of 10, 20 and 50 µm with a fixed spot size of 20 µm.

When photon counts are low, resulting in poor spectral statistics, binning of adjacent pixels is recommended to improve counting statistics. This behavior is clearly reflected in the table, where increasing pixel binning leads to a substantial reduction in QMAP processing time, particularly at smaller step sizes. At a 10 µm step size, limited counts per pixel cause excessively long processing times without binning, whereas applying 9 × 9 binning reduces the total analysis time by nearly an order of magnitude. Similar improvements are observed at 20 µm with increasing binning levels. At 50 µm, sufficient counts are achieved even with minimal binning, and the combination of coarse step size and 9 × 9 binning reduces QMAP processing to only a few minutes, resulting in a total scan time of less than 1 hour. Overall, Table 3 confirms that

Table 2

Measurement Duration and Total Acquisition Time for Micro-XRF Mapping of a 24 mm × 21 mm Area of the TS1-2 × 2 Sample as a Function of Step Size and QMAP Pixel Binning

Step size	Measurement duration (hrs.)	Pixel binning	Additional time for QMAP (hrs.)	Total time (hrs.)	Total time (mins.)
10 µm	8.5	1 × 1	90	98.5	5,910
		3 × 3	27	35.5	2,130
		5 × 5	7	15.5	930
		9 × 9	1.7	10.2	612
20 µm	4.15	1 × 1	26.7	30.85	1,851
		3 × 3	6.7	10.85	651
		5 × 5	1.67	5.82	349.2
		9 × 9	0.4	4.55	273
50 µm	0.8	1 × 1	4.3	5.1	306
		3 × 3	1	1.8	108
		5 × 5	0.3	1.1	66
		9 × 9	0.05 (3 mins!)	0.85	51

Figure 6

Comparison of manganese concentration line profiles measured by micro-XRF at various step sizes and pixel binning levels, with mean Mn values indicated for each condition.

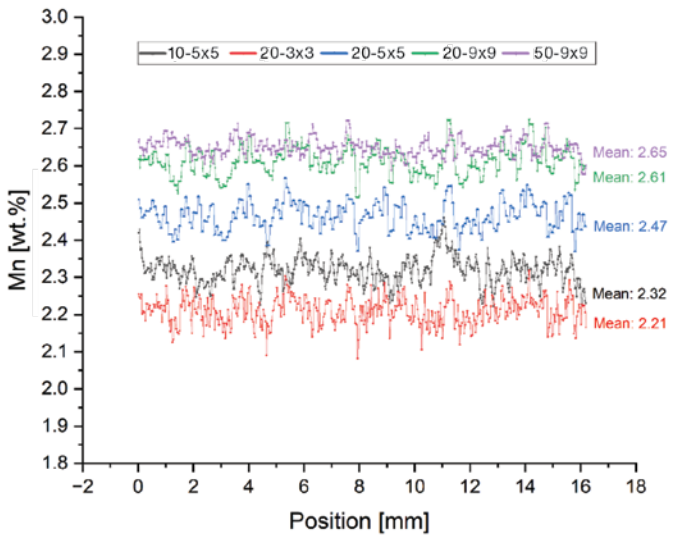

pixel binning is essential when count statistics are limited and demonstrates that appropriate binning selection is critical for achieving both reliable quantification and practical analysis times in large-area micro-XRF mapping.

Fig. 6 compares manganese concentration profiles extracted from micro-XRF line scans obtained using different combinations of step size and pixel binning at the same line. Each curve represents the Mn concentration measured along the same spatial line, with the average value for each condition indicated on the right. At the finest effective resolutions, i.e., very small step sizes and low binning (10 µm–5 × 5 and 20 µm–3 × 3), each pixel represents a very small interaction volume. As a result, only a limited number of Mn fluorescence photons are generated and detected per pixel. When photon counts are low, the signal is dominated by statistical (Poisson) noise. This may cause strong point-to-point fluctuations in the line profiles and may make peak fitting less stable. Under these conditions, weak or noisy Mn peaks are more likely to be underestimated, which pulls the average Mn concentration to lower values. As the step size and binning level increase (20 µm–5 × 5 and 20 µm–9 × 9), the profiles become progressively smoother and the mean Mn concentration increases, reflecting improved counting statistics and more stable quantification. The 50 µm–9 × 9 pixel binning condition yields the smoothest profile and the highest average Mn concentration (~2.65 wt. %), indicating that coarse step sizes combined with aggressive pixel binning provide sufficient photon statistics for reliable manganese quantification. Overall, the figure demonstrates that manganese quantification is highly sensitive to signal statistics and that increasing pixel binning and step size improves measurement stability and accuracy, making coarse-resolution scans a quick and suitable option for practical segregation analysis.

Figure 7

OES versus micro-XRF (M4) measurements of Mn and Si in the TS1-2 × 2 sample at 50 µm step size and 9 × 9 pixel binning.

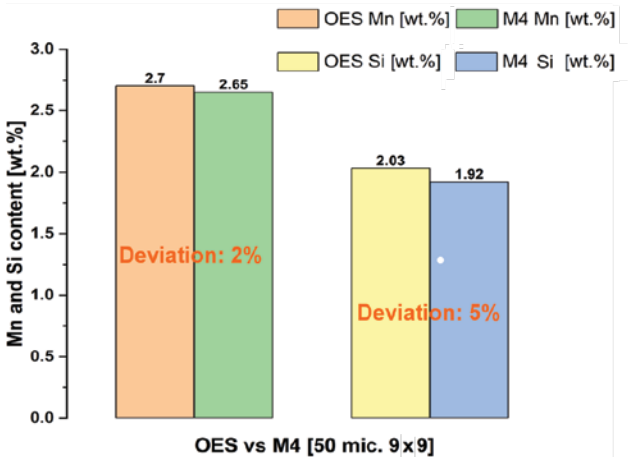

Because the 50 µm step size combined with 9 × 9 pixel binning provides both rapid acquisition and high quantitative accuracy, this condition is emphasized and explored in greater detail. Manganese, as a relatively heavy element with a high fluorescence yield and strong characteristic x-ray lines, shows excellent agreement between micro-XRF and OES even under these coarse acquisition parameters. As shown in Fig. 7, the manganese concentration measured by micro-XRF at 50 µm with 9 × 9 binning closely matches the OES reference measured along the corresponding opposite line, with a deviation of approximately 2%. This small deviation indicates that, despite the reduced spatial resolution, robust counting statistics are achieved, and noise is effectively suppressed without compromising accuracy.

These results confirm that optimized coarse-resolution scanning is adequate for reliable manganese segregation assessment (≈2.7 wt. %) in the TS1-2 × 2 sample. Silicon, as a lighter element with lower fluorescence yield and higher sensitivity to matrix absorption, shows slightly larger deviations than manganese. At a 50 µm step size with 9 × 9 pixel binning, the micro-XRF silicon concentration deviates from the OES reference by approximately 5%, as shown in Fig. 7. Although higher than for manganese, this deviation remains acceptable for segregation characterization and trend analysis. Overall, the results indicate that the selected acquisition parameters provide a practical balance between measurement throughput and quantitative reliability for both manganese and silicon in the TS1-2 × 2 sample.

Spatial Representation of Segregation Morphology

Fig. 8 compares manganese distribution in the TS1-2 × 2 sample (24 mm × 21 mm) obtained using different micro-XRF acquisition parameters, highlighting the trade-off between spatial detail and quantitative efficiency. The leftmost image presents the M4 mosaic of the analyzed region, serving as a reference for the mapped area. The Mn map acquired at 10 µm step size with 5 × 5 pixel binning resolves fine-scale segregation features more clearly. Localized Mn-enriched regions are readily identifiable, demonstrating improved segregation morphology and spatial detail. However, this condition requires longer acquisition and processing times and exhibits increased point-to-point noise due to limited photon counts per pixel. At 20 µm step size with 9 × 9 pixel binning, the Mn map shows reduced noise and smoother contrast while still preserving the main segregation features. Although some fine morphological detail is lost compared to the 10 µm scan, the dominant Mn-enriched regions remain clearly distinguishable as illustrated in black circles in

Figure 8

Micro-XRF Mn maps of the TS1-2 × 2 sample acquired with varying step sizes and pixel binning, highlighting improved segregation morphology at finer resolution and faster, more uniform results at coarser resolution. Note: Scale bar length varies between panels due to differences in step size and display scaling, although the scanned area is identical.

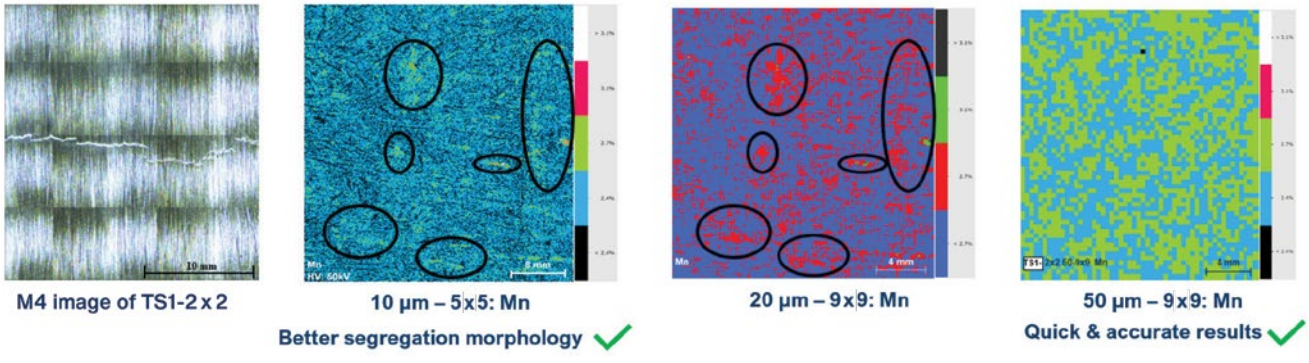

Figure 9

Comparison of OES reference compositions and micro-XRF (M4) measurements for Mn, Si and Al in the TS12 sample obtained using a 50 µm step size with 9 × 9 pixel binning, showing deviations of ~4% for Mn, ~12% for Si, and ~15% for Al.

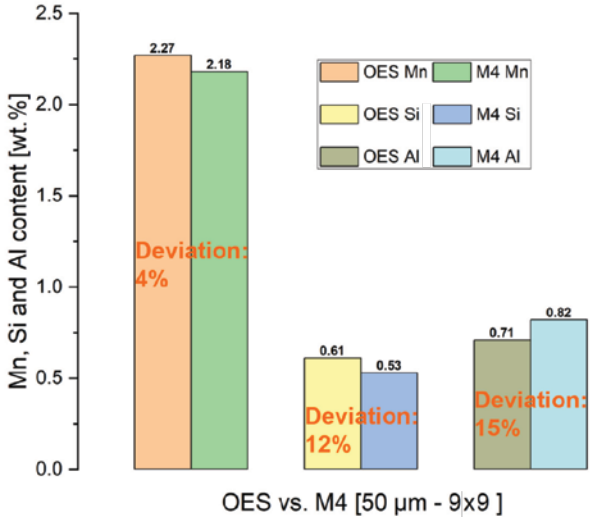

Figure 10

Method editor view illustrating the application of element-specific quantification correction factors for Mn, Si and Al in the TS12 sample using the fundamental parameter (FP) approach.

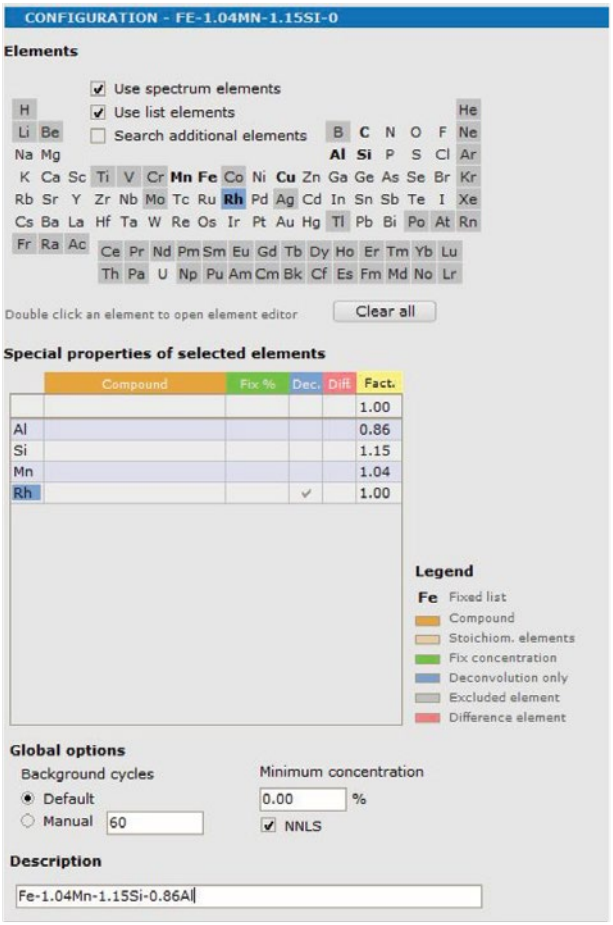

Fig. 8, indicating improved signal statistics and more stable quantification. As demonstrated earlier, the 50 µm step size combined with 9 × 9 pixel binning yields the most uniform Mn map and enables rapid, robust quantification, albeit with reduced fine-scale morphological detail. While small-scale segregation features are averaged out, the overall Mn distribution and concentration level are accurately captured. This condition provides the fastest acquisition and processing time and yields reliable quantitative results, making it well suited for practical, large-area segregation assessment where throughput and accuracy are prioritized.

Limitations of Scan Parameter Optimization and Motivation for FP Quantification

To evaluate the robustness of the optimized acquisition parameters, the 50 µm step size with 9 × 9 pixel binning — previously identified as providing rapid and acceptably accurate results for Mn and Si — was applied to a second sample, TS12. The OES reference composition of this sample is 2.27 wt. % Mn, 0.61 wt. % Si and 0.71 wt. % Al; other trace elements were intentionally excluded, enabling direct assessment of both heavy and light alloying elements under identical conditions. As shown in Fig. 9, manganese exhibits excellent agreement between micro-XRF and OES, with a deviation of only ~4%, confirming that the selected coarse-resolution parameters remain reliable for Mn quantification across different compositions. In contrast, the lighter elements silicon and aluminum show higher deviations of approximately 12% and 15%, respectively.

The element-dependent discrepancies observed in Fig. 9 indicate that optimization of scan parameters alone does not ensure uniform quantitative accuracy for all alloying elements. To address this limitation, a modification of the FP-based quantification approach was adopted. The FP method relies on a physics-based relationship between measured x-ray intensities and elemental concentrations, derived from fundamental atomic constants governing x-ray generation and absorption. Unlike purely empirical calibration methods, FP quantification can be implemented in a standardless mode when elemental identification is the primary objective. As a result, the FP framework provides a more robust basis for correcting matrix- and absorption-related effects, which is particularly important for improving the accuracy of lighter element quantification.

Application of FP Quantification

To address the element-dependent deviations observed with scan-parameter optimization alone, a modification of FP-based quantification approach was applied. In this study, the method editor–based FP quantification workflow was used, and the approach was first implemented on the TS12 sample. Within the method editor, deviations between measured micro-XRF concentrations and reference values can be minimized by defining element-specific quantification correction factors. Using OES measurements as reference, individual correction factors were applied for manganese, silicon and aluminum in the TS12 sample, as illustrated in Fig. 10.

This step allows systematic offsets in elemental response to be corrected while preserving the underlying physics-based FP framework. Following method optimization, QMAP quantification was repeated on the same TC12 sample using the previously optimized acquisition parameters of 50 µm step size with 9 × 9 pixel binning, now incorporating the modified FP method. As shown in Fig. 11, the application of FP correction resulted in a substantial reduction in deviation for all three elements. Manganese and silicon achieved 100% agreement with OES reference values, while aluminum exhibited a residual deviation of approximately 3%. Although aluminum remains the most challenging element due to its low atomic number, this level of deviation is considered acceptable for macrosegregation analysis in a chemically homogeneous steel such as TS12. For comparison, prior to FP correction, deviations of approximately 4% for Mn, 12% for Si and 15% for Al were observed under identical acquisition conditions, as discussed earlier and shown in Fig. 9. The results demonstrate that while step size and pixel binning optimization significantly improve quantitative stability, FP-based correction is essential for achieving high quantitative accuracy across both heavy and light alloying elements.

This saved FP-based quantification method was subsequently applied to another material of similar composition, MN1, containing 2.22 wt. % Mn, 0.60 wt. % Si and 0.63 wt. % Al, as determined by OES (trace elements excluded). As shown in Fig. 12, manganese again exhibits excellent agreement between micro-XRF and OES, with essentially zero deviation, confirming the robustness and transferability of the FP-corrected method for heavy alloying elements across different steel chemistries.

Silicon also shows improved accuracy compared to uncorrected results, with a deviation of approximately 3%, indicating that the FP approach effectively compensates for matrix-related effects for this element. Aluminum exhibits a slightly higher deviation of approximately 8%, which, although larger than for Mn and Si, represents a substantial improvement over the uncorrected case and remains acceptable for macrosegregation analysis in homogeneous steel samples such as MN1. Overall, these results demonstrate that the FP quantification method calibrated on TS12 can be reliably applied to chemically similar steels, providing consistent improvements in quantitative accuracy, particularly for lighter alloying elements.

The leftmost Bruker M4 mosaic image in Fig. 13 shows the etched surface of MN1 sample of the area of

Figure 11

Comparison of OES reference compositions and micro-XRF (M4) measurements for Mn, Si and Al in the TS12 sample after applying FP-based quantification using a 50 µm step size and 9 × 9 pixel binning.

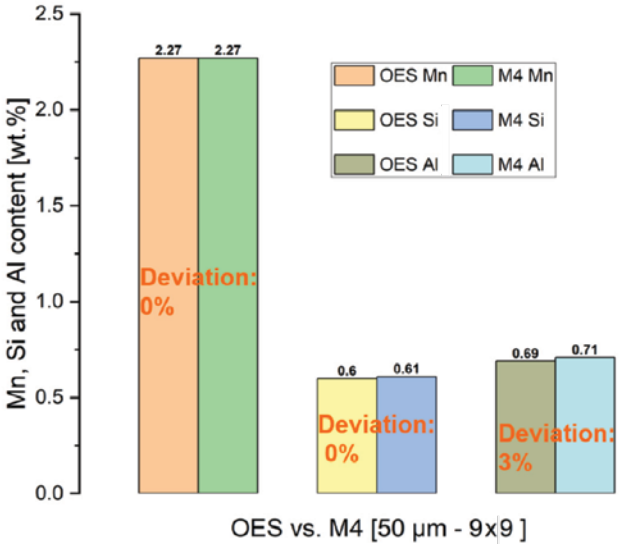

Figure 12

Comparison of OES reference compositions and micro-XRF (M4) measurements for Mn, Si and Al in the MN1 sample after applying FP-based quantification using a 50 µm step size and 9 × 9 pixel binning.

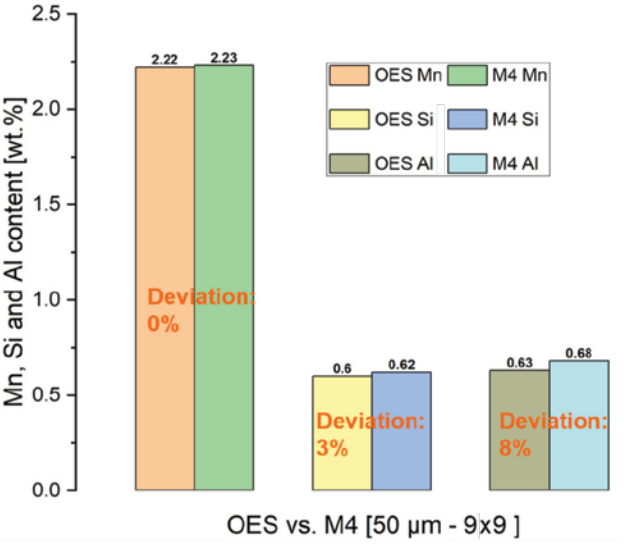

Figure 13

Comparison of manganese distribution maps for the MN1 sample obtained using different micro-XRF acquisition parameters. The etched surface (left) is shown for reference, while Mn maps acquired at 20 µm–3 × 3 and 50 µm–9 × 9 with modified FP method illustrate the trade-off between spatial resolution and processing efficiency, with finer resolution capturing detailed segregation morphology and coarser resolution enabling rapid, robust quantification.

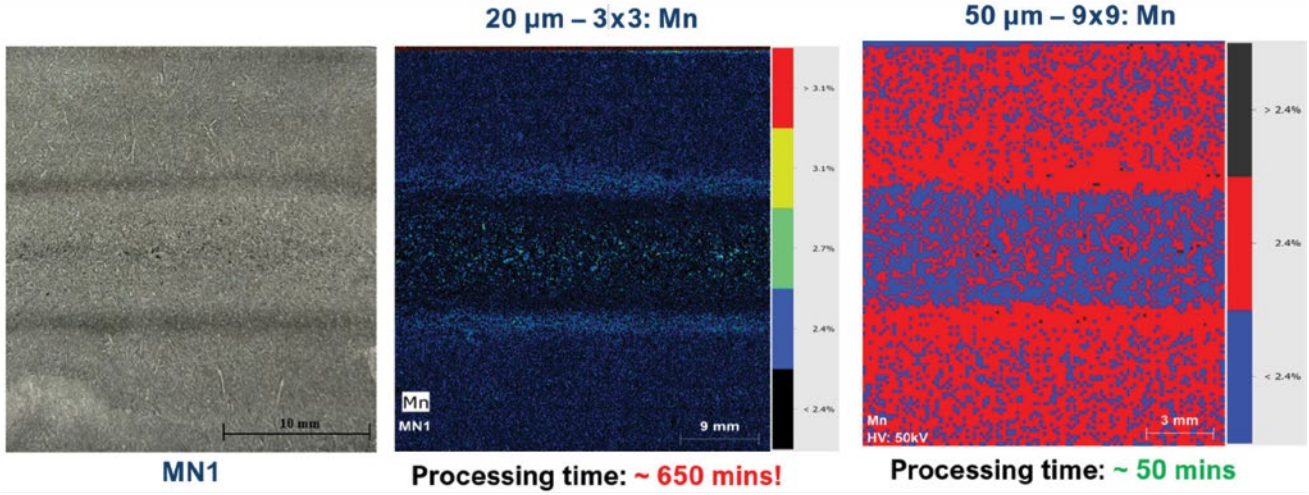

24 mm × 21 mm. The manganese map obtained at a 20 µm step size with 3 × 3 pixel binning, when processed using the FP-based quantification method, provides enhanced spatial resolution and resolves finer-scale segregation features more distinctly. Under these conditions, banded segregation patterns across the analyzed region are clearly visible, allowing improved visualization of local Mn-enriched and Mn-depleted zones, i.e., positive and negative segregation bands. At this higher spatial resolution, the Mn segregation pattern shows good correspondence with the features observed on the etched surface. This higher spatial accuracy is achieved because the smaller step size preserves detailed chemical variations associated with solidification and macrosegregation phenomena, and results in substantially longer QMAP processing time, approximately 650 minutes. This condition, while offering higher spatial detail, is less practical for large-area analysis due to its extended processing requirements. In contrast, while fine-scale morphological detail is averaged out in the Mn map acquired at a 50 µm step size with 9 × 9 pixel binning, the dominant segregation bands remain clearly discernible. Notably, the processing time is reduced to approximately 50 minutes, corresponding to more than an order-of-magnitude improvement in efficiency.

Fig. 14 shows the manganese concentration profile extracted along the thickness direction of the MN1 sample obtained using micro-XRF at a 50 µm step size with 9 × 9 pixel binning and the modified FP-based method. The background grayscale image corresponds to the mosaic image of the analyzed region, providing spatial context for the line scan. The black curve represents the local Mn concentration as a function of distance through the slab thickness, while the horizontal black line indicates the average manganese content. The profile reveals a clear segregation pattern across the thickness, characterized by a central Mn-depleted region flanked by Mn-enriched

Figure 14

Through-thickness manganese concentration profile of the MN1 sample obtained by micro-XRF using a 50 µm step size with 9 × 9 pixel binning and the modified FP-based quantification method, showing alternating Mn-enriched and Mn-depleted segregation bands along with centerline segregation.

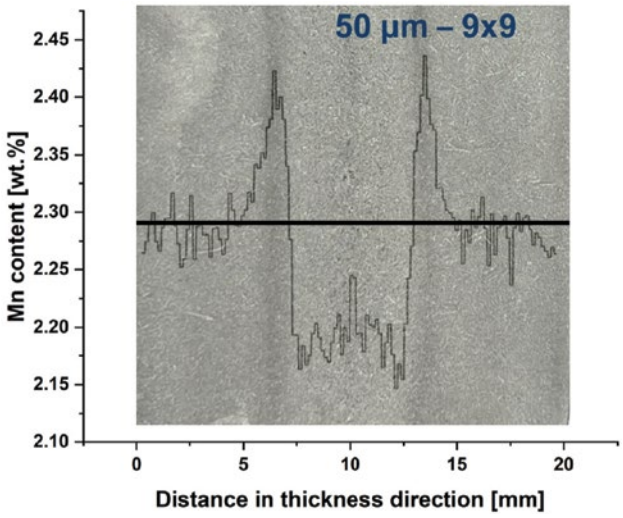

bands on either side. Despite the coarse spatial resolution, the dominant segregation trend is clearly captured, demonstrating that the selected acquisition parameters provide sufficient sensitivity to resolve macroscopic chemical variations. Minor point-to-point fluctuations are present but remain limited, reflecting improved counting statistics achieved through high pixel binning. Overall, the figure confirms that micro-XRF mapping at 50 µm step size with 9 × 9 pixel binning is capable of rapidly and reliably capturing through-thickness manganese segregation profiles, making it suitable for large-area macrosegregation analysis.

The remaining ~8% deviation observed for aluminum may primarily be due to the inherent challenges of quantifying low-Z elements in micro-XRF. Aluminum has a low fluorescence yield and emits low-energy x-rays that are strongly absorbed by the steel matrix, making its measurement more prone to uncertainty. In addition, the presence of other alloying elements such as Cr, Ti, Mo, Ni and Cu can influence Al fluorescence through interelement effects and increased background, complicating peak deconvolution. While the modified FP method significantly reduces these effects, some residual deviation can remain as the number of alloying elements

Figure 15

(a) Mosaic image of sample TS156 obtained using the Bruker M4 micro-XRF system, showing the central liquid pool at the center of the concentric solidification sample used in confocal laser scanning microscope (CLSM); (b) Mn concentration map of the sample TS156 obtained by QMAP quantification (50 µm step size, 9 × 9 binning) using the modified FP method; (c) In-situ CLSM image showing MnS precipitation at ~1,435°C during cooling under liquid and austenite coexistence; and (d) S concentration map of sample TS156 obtained by QMAP quantification, showing localized enrichment in the last solidified region.

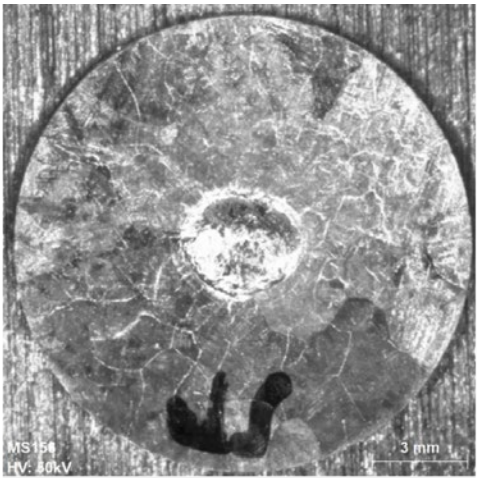

(a)

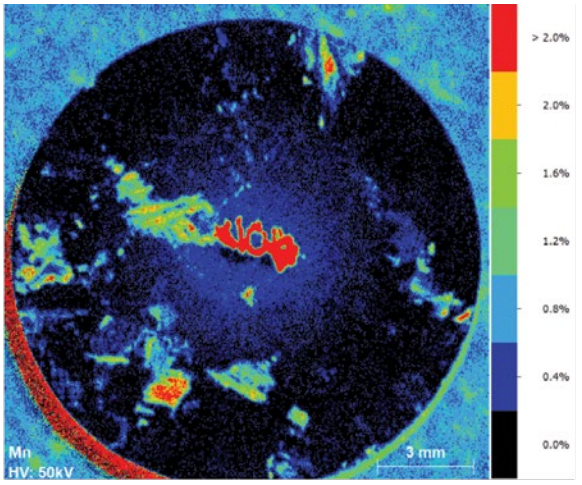

(b)

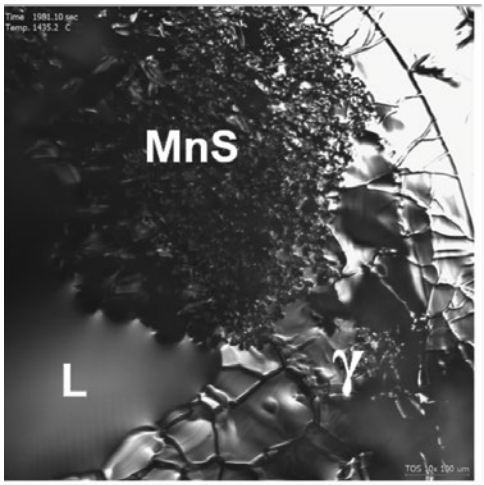

(c)

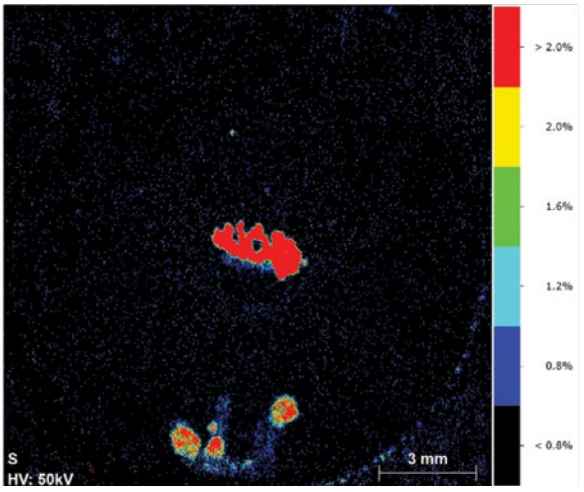

(d)

and their concentration ranges increase, indicating that further method adjustment may be required for improved Al accuracy.

Validation of Micro-XRF Elemental Quantification Using CLSM and SEM-EDS

The capability of the Bruker M4 Tornado micro-XRF system to quantify elemental segregation was validated using complementary CLSM and SEM-EDS analyses on sample TS156 from the concentric solidification experiment. The mosaic image in Fig. 15a clearly reveals the circular solidification morphology, with the central liquid pool corresponding to the last solidified region. Elemental mapping was performed using QMAP quantification with a 50 µm step size, 9 × 9 pixel binning, and a modified FP method. The Mn map in Fig. 15b shows pronounced enrichment at the center of the sample, consistent with solute redistribution toward the final liquid during solidification. The S map exhibits similar localized enrichment in the same region as shown in Fig. 15d, indicating coupled Mn–S segregation. In-situ CLSM observations confirm that MnS precipitation occurs at approximately 1,435°C during cooling, when liquid and austenite (γ) phases coexist, as illustrated in Fig. 15c. This directly supports the compositional enrichment detected by micro-XRF. SEM imaging of the central region reveals discrete precipitates within the last solidified zone, and EDS mapping in Fig. 16 confirms strong spatial overlap between Mn and S, verifying MnS formation with minor dispersed carbides.

The agreement among micro-XRF QMAP results, in-situ CLSM precipitation observations, and SEM-EDS elemental mapping demonstrates that the Bruker M4 system, combined with the modified FP approach, reliably

Figure 16

(a) Scanning electron microscopy (SEM) backscattered image of the central region showing precipitate morphology, (b) SEM-energy-dispersive x-ray spectroscopy (EDS) elemental mapping confirming MnS precipitation with minor dispersed carbides, (c) Individual Mn elemental map from SEM-EDS analysis, and (d) Individual S elemental map from SEM-EDS analysis showing spatial correlation with Mn.

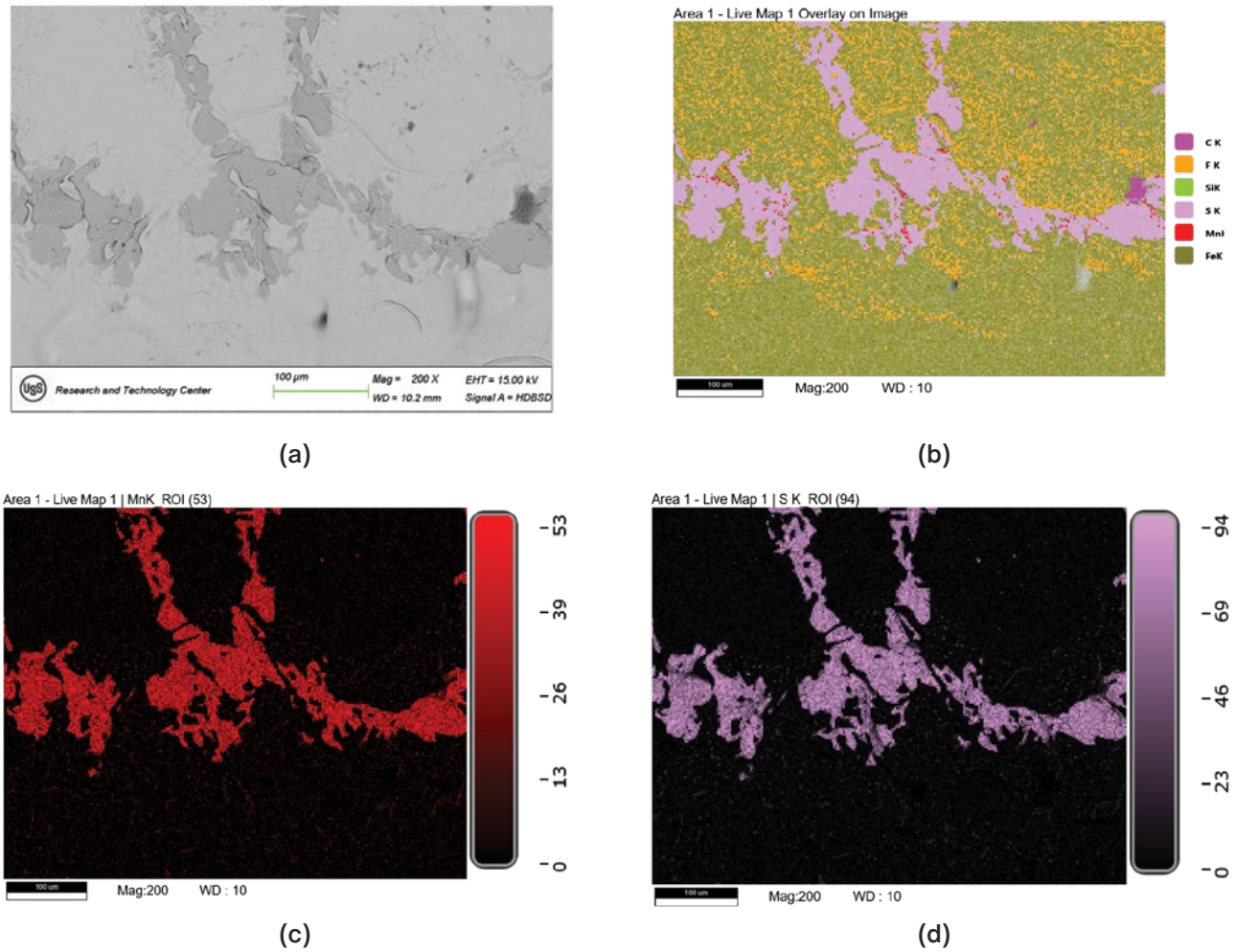

captures segregation at a spatial scale consistent with microstructural features. These results validate laboratory-based micro-XRF as an effective tool for quantitative segregation assessment in solidified steel.

Conclusions

Micro-XRF combined with QMAP and FP-based quantification provides an effective, nondestructive method for quantitative characterization of centerline macrosegregation in steel slabs. A scanning strategy employing a 50 µm step size with 9 × 9 pixel binning offers the best compromise between accuracy, spatial relevance and processing time. FP correction significantly improves quantification of lighter elements such as Si and Al, enabling multielement segregation analysis. The developed methodology offers a practical alternative to conventional destructive techniques and can support both research studies and industrial quality evaluation. The quantitative micro-XRF capabilities were further validated through in-situ CLSM observations and SEM-EDS mapping of MnS precipitation. Future work will focus on developing a comprehensive segregation matrix for Mn, Si and Al, while extending the methodology to accommodate additional alloying elements such as Co, Ni, Ti, Nb and V.

Acknowledgments

This work was sponsored and carried out at the U. S. Steel Research and Technology Center, Munhall, Pa., USA. The authors gratefully acknowledge the support and resources provided by the research center.

References

1. G. Krauss, "Solidification, Segregation, and Banding in Carbon and Alloy Steels," *Metallurgical and Materials Transactions B,* Vol. 34, No. 6, 2003, pp. 781–792, DOI: 10.1007/s11663-003-0084-z.
2. G. Lesoult, "Macrosegregation in Steel Strands and Ingots: Characterization, Formation and Consequences," *Materials Science and Engineering A,* Vol. 413–414, 2005, pp. 19–29, DOI: 10.1016/j.msea.2005.08.203.
3. T.J. Piccone, T.T. Natarajan, S.R. Story, B. Jones and D.M. Hreso, "Quantitative Methods for Evaluation of Centerline Segregation," *AISTech 2016 Conference Proceedings,* 2016.
4. S. Abraham, J. Cottrell, J. Raines, Y. Wang, R. Bodnar, S. Wilder, J. Thomas and J. Peters, "Development of an Image Analysis Technique for Quantitative Evaluation of Centerline Segregation in As-Cast Products," *Iron & Steel Technology,* Vol. 14, No. 8, 2017, pp. 148–157.
5. J. Sengupta, J. Leung and K. Witherspoon, "Bridging the Gap: MXRF Technique Rapidly Maps Centerline Segregation," *Iron & Steel Technology,* Vol. 7, 2017, pp. 66–74.
6. Classification of Defects in Materials — Standard Charts and Sample Guide, SMS Demag, 2009.
7. F. Boué-Bigne, "Simultaneous Characterization of Elemental Segregation and Cementite Networks in High Carbon Steel Products by Spatially Resolved Laser-Induced Breakdown Spectroscopy," *Spectrochimica Acta Part B,* Vol. 96, 2014, pp. 21–32, DOI: 10.1016/j.sab.2014.03.011.
8. S.K. Choudhary, S. Ganguly, A. Sengupta and V. Sharma, "Solidification Morphology and Segregation in Continuously Cast Steel Slab," *Journal of Materials Processing Technology,* Vol. 243, 2017, pp. 312–321, DOI: 10.1016/j.jmatprotec.2016.12.030.
9. X. Wu, J. Zhang, F. Guo, R.D.K. Misra, X. Wang and X. Li, "Deep Learning-Based Automatic Recognition of Segregation in Continuous Casting Slabs," *Metals,* Vol. 15, No. 12, 2025, p. 1380, DOI: 10.3390/met15121380.
10. M. Halstead, Laser Ablation ICP-MS Analytical Report: Analysis of Steel, Technical Report, 2012.
11. A. Al Rafi, B. Santillana, R. Feng, B.G. Thomas and A.B. Phillion, "Analysis of Microscopy Techniques to Measure Segregation in Continuous-Cast Steel Slabs," *Journal of Microscopy,* Vol. 295, No. 3, 2024, pp. 266–277, DOI: 10.1111/jmi.13310.
12. Type Calibrations and Method Editing for Quantification in the M4, Training Manual, Bruker Corp., 2021.
13. J. Sengupta, J. Leung and A. Noorafkan, "Calibration and Validation of X-Ray Fluorescence Technique for Mapping Centerline Segregation on Steel Slabs," *AISTech 2017 Conference Proceedings,* 2017.
14. Bruker Micro-XRF Application Team, Introduction to MQuant and Fundamental Parameter Quantification in the M4 TORNADO, Bruker Corp., 2023.

AISTech This paper was presented at AISTech 2026 — The Iron & Steel Technology Conference and Exposition, Pittsburgh, Pa., USA, and published in the AISTech 2026 Conference Proceedings.